International Journal of Nanomedicine

Dovepress
open access to scientific and medical research

Open Access Full Text Article

ORIGINAL RESEARCH

Iron–gold alloy nanoparticles serve as a cornerstone in hyperthermia-mediated controlled drug release for cancer therapy

This article was published in the following Dove Press journal:
International Journal of Nanomedicine

Yun-Qian Li,[1,*] Meng Xu,[2,*] Udesh Dhawan,[3,4] Wai-Ching Liu,[5] Kou-Ting Wu,[5] Xin-Rui Liu,[1] Chingpo Lin,[1] Gang Zhao,[1] Yu-Chuan Wu,[3,6,7] Ren-Jei Chung[5]

[1]Department of Neurosurgical Oncology, First Hospital, Jilin University, Changchun, People's Republic of China; [2]School of Materials Science and Engineering, Beijing Institute of Technology, Beijing, People's Republic of China; [3]Department of Materials and Mineral Resources Engineering, National Taipei University of Technology (Taipei Tech), Taipei, Taiwan, Republic of China; [4]Institute of Chemistry, Academia Sinica, Taipei, Taiwan, Republic of China; [5]Department of Chemical Engineering and Biotechnology, National Taipei University of Technology (Taipei Tech), Taipei, Taiwan, Republic of China; [6]Institute of Materials Science and Engineering, National Taipei University of Technology (Taipei Tech), Taipei, Taiwan, Republic of China; [7]Department of Chemical and Materials Engineering, Chinese Culture University, Taipei, Taiwan, Republic of China

*These authors contributed equally to this work

Correspondence: Yu-Chuan Wu
Department of Materials and Mineral Resources Engineering, National Taipei University of Technology (Taipei Tech), No 1, Section 3, Zhongxiao East Road, Taipei 10608, Taiwan, Republic of China
Tel +886 2 2771 2171 ext 2765
Email wuyc@mail.ntut.edu.tw

Ren-Jei Chung
Department of Chemical Engineering and Biotechnology, National Taipei University of Technology (Taipei Tech), No 1, Section 3, Zhongxiao East Road, Taipei 10608, Taiwan, Republic of China
Tel +886 2 2771 2171 ext 2547
Email rjchung@ntut.edu.tw

Introduction: The efficacy of a chemotherapy drug in cancer therapy is highly determined by the ability to control the rate and extent of its release in vivo. However, the lack of techniques to accurately control drug release drastically limits the potency of a chemotherapy drug.

Materials and methods: Here, we present a novel strategy to precisely monitor drug release under magnetic stimulation. Methotrexate (MTX), an anticancer drug, was covalently functionalized onto iron–gold alloy magnetic nanoparticles (Fe–Au alloy nanoparticles or NFAs) through 2-aminoethanethiol grafting and the ability of this drug–nanoparticle conjugate (NFA–MTX) in limiting HepG2 (liver carcinoma) cell growth was studied. Well-dispersed NFAs were prepared through pyrolysis.

Results and discussion: Transmission electron microscopy revealed the average nanoparticle size to be 7.22±2.6 nm, while X-ray diffraction showed distinct 2θ peaks for iron and gold, confirming the presence of iron and gold nanoparticles. Inductively coupled plasma mass spectrometry revealed that the amount of NFA–MTX conjugate ingested by HepG2 cancer cells was 1.5 times higher than that ingested by L929 fibroblasts, thereby proving a higher selective ingestion by cancer cells compared to normal cells. Fourier-transform infrared spectroscopy revealed the breakage of Au–S bonds by the heat generated under magnetic field stimulation to release MTX from the NFA–MTX conjugate, triggering a 95% decrease in cellular viability at 100 µg/mL.

Conclusion: The ability of NFA–MTX to dissociate under the influence of an applied magnetic field provides a new strategy to induce cancer cell death via hyperthermia. Applications in drug delivery, drug development, and cancer research are expected.

Keywords: iron–gold nanoparticles, methotrexate, hyperthermia, superparamagnetic, controlled drug release

Introduction

Nanotechnology has recently emerged as an indispensable area of research, with applications in all fields of science. Nanoparticles, in particular, have revolutionized the medical industry by finding applications in pharmaceutics,[1] diagnostics,[2] and drug delivery.[3] This is specifically due to the size-dependent variation in the properties of nanoparticles,[4] allowing them to display different physical and chemical behaviors under varying conditions. Single metal as well as metal alloy nanoparticles are exploited in the fields of catalysis,[5] imaging,[6] and biomedical[7] or tissue engineering.[8,9] A variety of nanoparticles such as gold, titania, silica, iron, and zinc sulfide have found applications in immunocytochemistry,[10] antibacterial medications,[11] fluorescent dyes,[12] drug delivery,[13,14] and biological imaging,[15] respectively. Additionally, the

submit your manuscript | www.dovepress.com
Dovepress
http://dx.doi.org/10.2147/IJN.S163721

nano size of these particles makes it easier for them to be ingested by cells, where they can conveniently interact with cellular components and provide useful information about biological processes.

Cancer continues to be the leading cause of death in both developing and developed countries, with an estimated 595,690 deaths in 2016 in the USA alone.[16] During the progress of cancer, the affected cells become resistant to antigrowth signals,[17] resulting in uncontrolled division. Such cells also show an increase in migration and invasion potential,[18] which may possibly lead to the establishment of fresh cancer colonies throughout the body. Various methods such as radiotherapy and chemotherapy have been proposed to induce cell apoptosis and limit cancer cell multiplication. Different cancer types display different characteristics because of variations in the cellular population, thereby rendering a single drug ineffective against multiple cancers. This complicates the already challenging task of limiting cancer metastasis. Furthermore, while the nonspecific distribution of chemotherapy drugs in vivo, accompanied with rapid clearance, significantly limits the drug potency, administering drugs at higher dosage is undesirable as it often poses a serious cytotoxic threat. To overcome the conventional drawbacks of chemotherapy, a variety of drug carriers such as polymeric nanoparticles,[19] polymeric micelles,[20] dendrimers,[21] liposomes,[22] magnetic nanoparticles (MNPs),[23] and silica[24] or gold nanoparticles[25] have been used to achieve targeted drug delivery (TDD).

MNPs have gained considerable attention in recent years because of their superparamagnetic nature,[26] finding applications in gene delivery,[27] contrast-enhancing agents,[28] tissue repair,[29] and bioseparation.[30] However, one of the key areas of MNP application lies in drug delivery, whereby a chemotherapy drug can be covalently functionalized onto MNPs, followed by its delivery to a specific site of action. This is due to the ease of functionalization of drug molecules onto MNPs, after which they can be magnetically guided to the site of action, making them ideal candidates for TDD. A major benefit of TDD is that it ensures the safety of healthy cells or tissues surrounding the diseased stroma.

Another technique to limit cancer cell growth is hyperthermia, which triggers cell death through necrosis and apoptosis.[31] Recent studies have suggested that hyperthermia may actually enhance the immune system to keep the growth of cancer cells in check.[32] However, insufficient understanding of the mechanisms of hyperthermia-induced cell death and the inability to directly target cancer tissue are the main reasons for the inefficacy of hyperthermia techniques as a primary tool for cancer therapy. An interesting yet unexplored alternative to hyperthermia in cancer therapy is the use of heat generated by MNPs under the influence of a magnetic field, which induces the release of chemotherapy drugs from the drug–MNP conjugate, ultimately triggering cancer cell death. This technique may act as a cornerstone in the use of hyperthermia for cancer therapy, whereby the magnetic field strength can be modulated to control the amount of drug release and ultimately improve the chemotherapeutic drug potency. Our previous study showed the potential of iron–gold (Fe–Au) alloy nanoparticles (NFAs) to induce hyperthermia. We reported the generation of 1.33×10^6 J of heat by each NFA when exposed to high-frequency induction wave (HFIW).[33] The lone NFAs showed no signs of toxicity up to a concentration of 10 mg/mL. However, under the influence of HFIW, NFAs triggered cell death via hyperthermia.

The present study is based on the hypothesis that the hyperthermic property of NFAs can be further exploited to trigger drug release from the NFA–drug conjugate, providing an additional way to achieve controlled drug release and thus ultimately improving the chemotherapeutic drug's efficacy in limiting cancer cell growth. To achieve this, methotrexate (MTX), a chemotherapy drug, was covalently functionalized onto NFA via 2-aminoethanethiol grafting, and the effect of an external magnetic field on drug release was studied. The selectively higher absorption of the NFA–MTX conjugate by cancer cells in contrast to that by normal fibroblasts was also reported. According to our results, the application of an external magnetic field can induce the degradation of the NFA–MTX conjugate. This leads to the active release of MTX, which is then selectively ingested by cancer cells, eventually triggering cell death. Thus, the ability of this NFA–drug conjugate to degrade as a function of the applied magnetic field provides an alternate way of utilizing hyperthermia in cancer therapy and presents a possible application of NFAs as drug carriers. Applications in cancer research, biomedical engineering, and drug delivery are expected.

Materials and methods

Materials

Dulbecco's Modified Eagle Medium (DMEM), minimum essential medium alpha modification (α-MEM), and fetal bovine serum (FBS) were purchased from Gibco (Thermo Fisher Scientific, Waltham, MA, USA). Ferrous sulfate 7-hydrate and toluene were purchased from Echo Chemical (Taiwan). Didecyldimethylammonium bromide, sodium borohydride, hydrogen tetrachloroaurate, and 3-mercapto-1-propanesulfonic acid were purchased from Sigma-Aldrich

Co (St Louis, MO, USA). Absolute ethanol was purchased from J.T. Baker (Taiwan). All other chemicals of analytical grade or higher were purchased from either Sigma or Merck (Whitehouse Station, NJ, USA).

Cell culture

L929 (mouse fibroblasts, American Type Culture Collection [ATCC], Manassas, VA, USA) and HepG2 (human hepatocellular carcinoma, ATCC) cells were cultured in DMEM and α-MEM, respectively, supplemented with 10% FBS, 100 U/mL penicillin, and 100 µg/mL streptomycin. Cell cultures were maintained in an incubator at 37°C at 95% humidity with 5% CO_2.

Preparation of NFAs

NFAs were prepared using the pyrolysis method, as described elsewhere.[33] Briefly, the solvents were passed over nitrogen to remove residual oxygen. Dimethylammonium bromide (0.352 g) was dissolved in 20 mL of toluene and heated to 110°C under continuous stirring for 15 min. Iron sulfate heptahydrate (0.0556 g) dissolved in 0.5 mL of deionized (DI) water was then briskly added to the solution. After 2 min, 1.5 mL of 2 M sodium borohydride was added to the above solution. After another 20 min, 1.5 mL of gold chloride solution (0.034 g of gold (III) chloride trihydrate and 0.5346 g of 3-mercapto-1-propanesulfonic acid, sodium salt) was added to the above solution. When the color of the above solution turned red, 1.5 mL of 2 M sodium borohydride was again added. The color of the solution turned purple and slowly faded. The solution was stirred for 30 min, after which 0.5 mL of 2 M aqueous sodium borohydride was added. The solution was kept at 84°C for 3 h.

Purification of NFAs

The synthesized NFAs were mixed with ethanol and centrifuged at 7,000 rpm for 15 min. The precipitate was washed several times with ethanol and chloroform. The dark-green solid sample was collected, dried in vacuum for 10 h, and finally placed in the presence of a magnetic field for magnetic separation. The magnetically induced portion was collected and characterized.

Characterization of NFAs

Transmission electron microscopy (TEM; JEM-1230; JEOL, Tokyo, Japan) and dynamic light scattering (DLS) were used to characterize the size and morphology of the NFAs, while the crystalline phases were identified using X-ray powder diffraction (XRD; Shimadzu XRD-6000; Shimadzu Corporation, Kyoto, Japan). The nanoparticle size was calculated by analyzing the TEM images using ImageJ. At least 50 measurements were taken to calculate the average nanoparticle size. The zeta potential was measured using Malvern Zetasizer Nano ZS90 (Malvern Instruments, Malvern, UK). Laser light of 660 nm was used for the analysis.

MTX functionalization onto NFAs

MTX was covalently attached onto NFAs using a two-step functionalization process. In the first step, 1 mg of NFAs and 10 mg of 2-aminoethanethiol were mixed in anhydrous alcohol (ethanol). The mixture was subjected to ultrasonication for 24 h at 40°C–50°C. The product was then washed three times with ethanol and purified. Fourier-transform infrared spectroscopy (FTIR) was used to detect and confirm the functionalization of 2-aminoethanethiol onto NFAs. In the second step, MTX was first dissolved in 17 mL of dimethyl sulfoxide to form solution A. Subsequently, 1-ethyl-3-(3-dimethylaminopropyl) carbodiimide hydrochloride (75 mM) and *N*-hydroxysuccinimide (15 mM) were dissolved in 17 mL of DI water to form solution B. Solutions A and B were mixed together, the pH was adjusted to 8.2, and 5 mg of NFAs was then added to the above mixture and incubated for 24 h. FTIR analysis was performed to confirm the functionalization of MTX onto the NFAs.

NFA–SH bond cleavage for drug release

To investigate the efficiency of an external magnetic field in cleaving the NFA–SH bond, which can trigger MTX release, 5 mg of NFA–SH was dispersed in 0.5 mL of DI water and placed in the presence of a high-frequency alternating current (AC) magnetic field for 20 min. The product was washed several times. FTIR was used to study the NFA–SH bond cleavage before and after magnetic stimulation.

Controlled drug release

NFA–MTX (2 mg) was dispersed in 5 mL of DI water and exposed to an AC magnetic field (frequency: 700–1,100 kHz) for different time durations (10, 20, and 30 min) to elucidate the effect of exposure time on MTX release from the NFA–MTX conjugate. NFA–MTX conjugates dispersed in DI water unexposed to the AC magnetic field were used as controls.

Study of NFA–MTX ingestion by cells

First, the NFA–MTX mixture was kept under ultraviolet (UV) light for 4 h to be sterilized. L929 and HepG2 cells were seeded at a density of 1×10^5 cells in a 6 cm Petri dish. The sterilized NFA–MTX mixture was added to the cells.

Cell cultures were maintained for 24 h, after which they were washed three times with 1 mL of RPMI serum-free medium, trypsinized, and dissolved in 1 mL of nitric acid. Inductively coupled plasma mass spectrometry (ICP-MS) was then performed to measure the iron ion concentration.

Cell viability

The cytotoxicity of NFA–MTX was studied using HepG2 cells, which were seeded in a 96-well plate at 1×10^4 cells per well. A fixed amount of NFAs (100 µL), varying dosages of NFA–MTX conjugate (0.1, 0.075, 0.05, 0.025, or 0.01 mg/mL), or MTX (0.01 mg/mL) alone were added to cells. The cells were cultured for 24 h and exposed to an AC magnetic field for 20 min. Five different experimental conditions were established at this point. Condition 1 consisted of cells cultured in NFAs. Condition 2 consisted of cells cultured in NFAs and exposed to a magnetic field for 20 min. Condition 3 consisted of cells cultured in NFA–MTX conjugates. Condition 4 consisted of cells cultured in NFA–MTX conjugates and exposed to a magnetic field for 20 min. Condition 5 consisted of cells in MTX only. After treatment, the cell culture medium was removed and the WST-8 assay (Sigma-Aldrich) was performed. WST-8 is a water-soluble tetrazolium salt used to assess cell metabolic activity. WST-8 solution (10 µL) was added and incubated for 4 h. Absorbance was then measured at 450 nm against a reference value at 630 nm and expressed as the relative absorbance using a microplate reader (Sunrise remote F039300; Tecan, Männedorf, Switzerland). Cells seeded in culture wells in standard medium were used as controls.

Statistics

All experiments were performed in triplicates, and data are expressed as mean ± SD. Unpaired-samples *t*-test (SPSS 17.0 software; SPSS Inc, Chicago, IL, USA) was used for statistical analysis, and the level of significance was set as $p<0.05$. Results from each group were first normalized with respect to the control group and then expressed as graphs.

Results and discussion

Characterization of NFAs

A schematic representation of the conjugation of NFA nanoparticles with MTX is shown in Figure 1. NFAs were

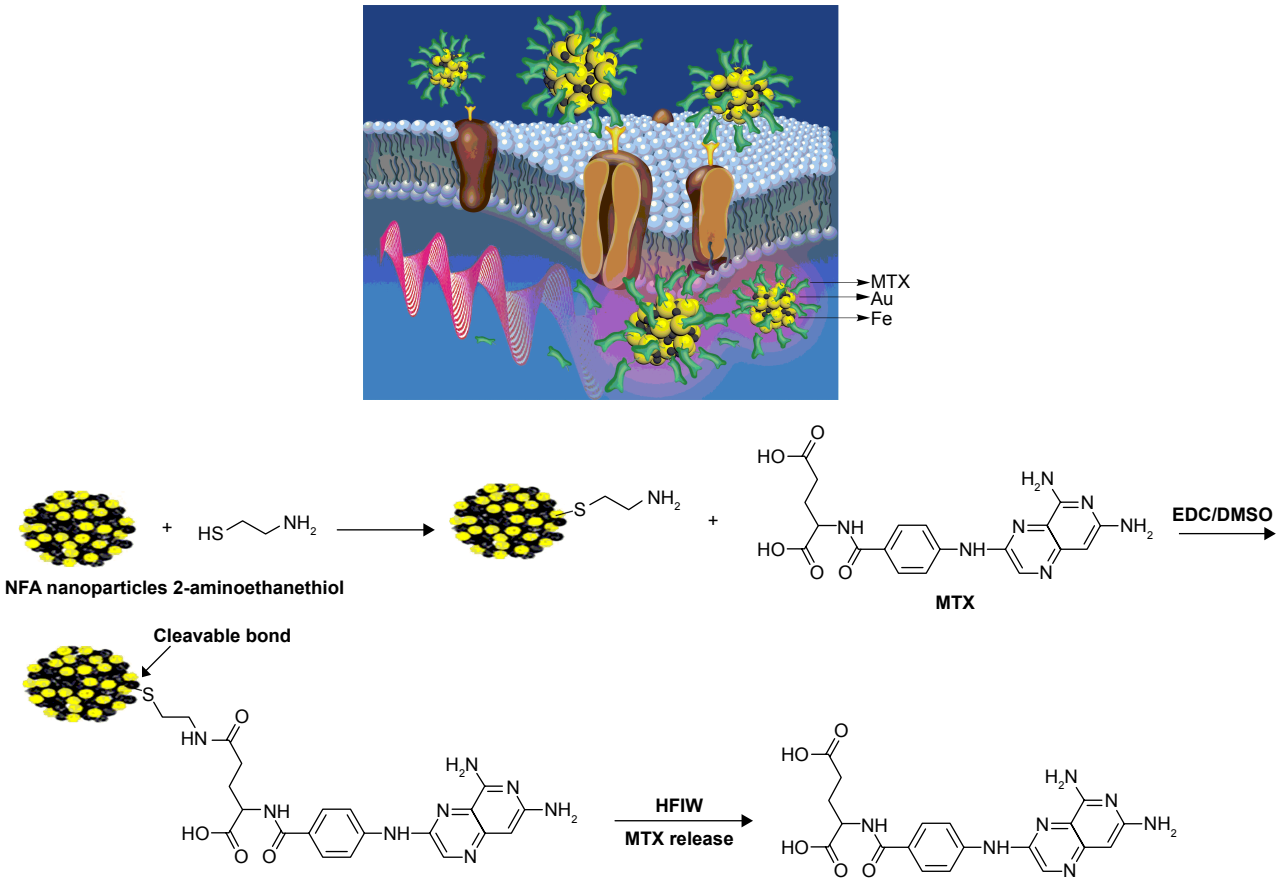

Figure 1 Schematic representation of MTX conjugation with NFA nanoparticles and its HFIW-mediated release.
Abbreviations: EDC, 1-ethyl-3-(3-dimethylaminopropyl)-carbodiimide; MTX, methotrexate; NFA, Fe–Au alloy nanoparticles; HFIW, high-frequency induction wave.

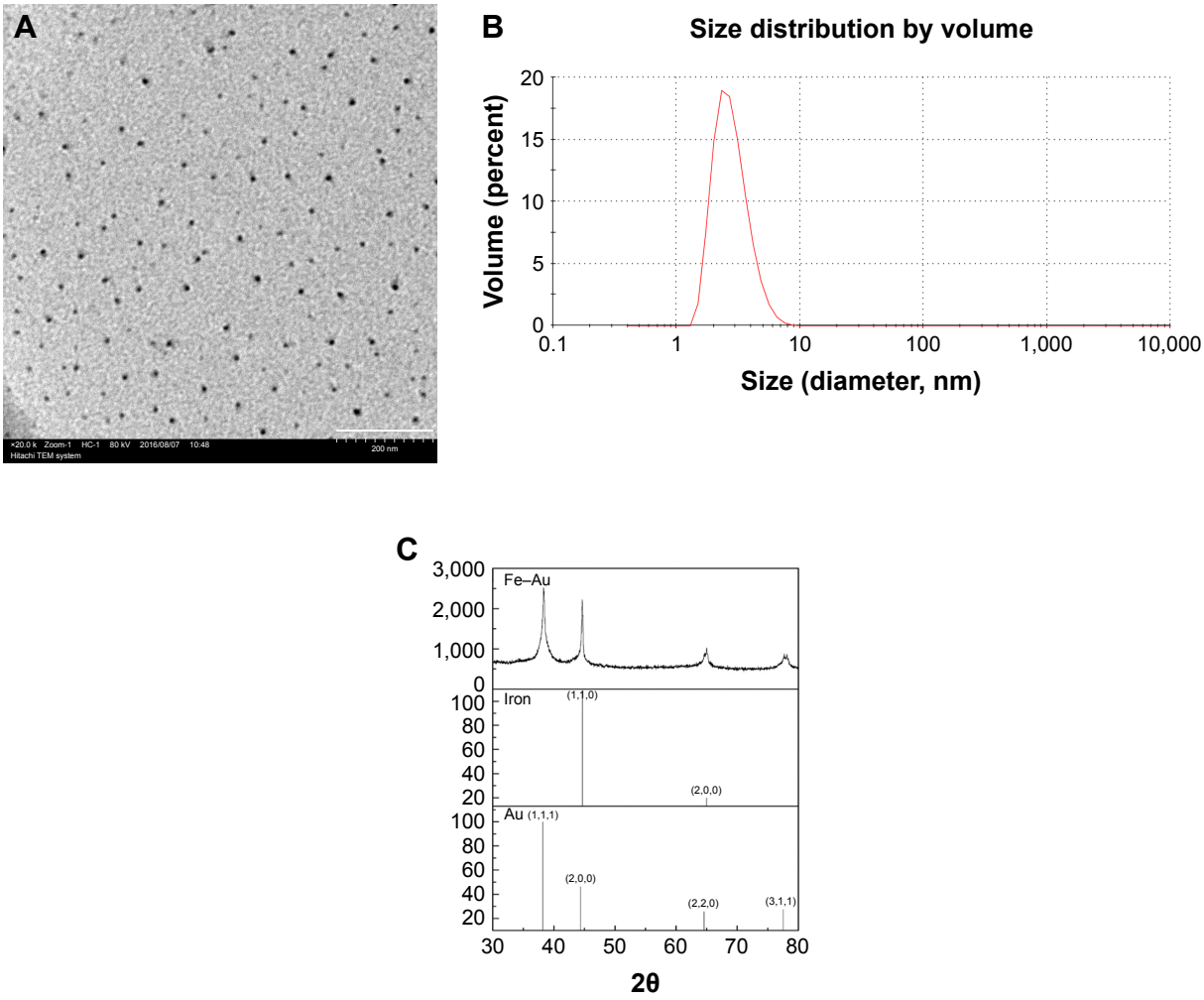

Figure 2 Characterization of NFAs.
Notes: (**A**) TEM image of NFAs (scale bar =200 nm). (**B**) DLS to analyze the size distribution of NFA nanoparticles. (**C**) XRD patterns of gold, iron, and resulting NFAs.
Abbreviations: NFA, Fe–Au alloy nanoparticles; TEM, transmission electron microscopy; DLS, dynamic light scattering; XRD, X-ray powder diffraction.

synthesized through the pyrolysis process using iron sulfate heptahydrate and hydrogen tetrachloroaurate as sources of iron and gold, respectively. TEM was used to analyze the morphology and size of the nanoparticles (Figure 2A), revealing that round NFAs had an average diameter of 2.8±0.95 nm (Figure 2B). In our previous study, we observed the average size of the NFA to be 3.9 nm.[33] A small difference in the alloy nanoparticle size may be attributed to a minute variation in the annealing temperature.[34] However, since there is no difference between the nanoparticles synthesized in this study and those in our previous study with respect to their composition, these nanoparticles were considered apt for further experiments. The estimated volume of the particles was 21.1 nm^3. XRD was used to analyze the crystal structure of the NFAs (Figure 2C). The (111), (200), and (220) planes of face-centered cubic gold were highlighted by the 2θ peaks at 38.67°, 44.81°, and 64.4°, respectively, while the (110) and (200) planes of the body-centered cubic iron were highlighted by the 2θ peaks at 43.9° and 64.8°, respectively (Figure 2C). The importance of the 2θ peaks lies in the fact that they reflect the crystal structure, as a transition in the peaks cannot only lead to a different crystal structure – which might trigger a change in the binding of NFAs with MTX – but also incite a different kind of behavior from the cellular entities. The 2θ peaks pertaining to different elements in the alloy nanoparticles were firmly consistent with the results of our previous study,[33] as well as with those obtained by Krishnamurthy et al,[35] thereby confirming the formation of NFAs. Furthermore, the absence of any arbitrary peaks also confirmed the purity of the NFAs.

An interesting aspect to consider at this point is the shape of the nanoparticles. Some studies have reported a modulation in the properties of nanoparticles with their shape.[36] Although the nanoparticles synthesized in the studies are single nanoparticles, it cannot be entirely ruled out that a modulation in the shape of NFAs may affect the amount of heat generated

under an applied magnetic field (AMF). Further experiments will be required to confirm this hypothesis.

Formation of NFA–MTX conjugate

FTIR was performed to confirm that MTX was successfully functionalized onto the NFAs. The FTIR spectra of unmodified NFAs and MTX-conjugated NFAs are shown in Figure 3A. NFA does not show any distinct peaks or bends because of the absence of any functional groups. The presence of C–N stretching between 1,350 and 1,000 cm^{-1} and N–H bending between 1,640 and 1,550 cm^{-1} confirmed that NFAs were successfully grafted with 2-aminoethanethiol (Figure 3A). MTX typically shows characteristic IR absorption peaks between 1,630 and 1,680 cm^{-1}, as reported by Kohler et al.[37] Thus, our results are consistent with those in the previous studies. The presence of a distinct MTX peak in the NFA–MTX mixed samples confirmed the conjugation of MTX onto NFAs.

Surface potential was also analyzed to further confirm NFA–MTX conjugation (Figure 3B). The amount of NH_3^+ present follows the trend NFA–MTX > NFA–SH > NFA. Since the presence of an acidic environment triggers the formation of NH_3^+, the maximum zeta potential was shown by NFA–MTX, confirming that MTX was successfully conjugated onto NFA.

Controlled drug release in the presence of an external magnetic field

One of the key factors limiting the applications of chemotherapy drugs is the lack of techniques to control their release. The uncontrolled release of a drug can be lethal to the nearby healthy tissues. Therefore, to overcome this issue, in the next step, we analyzed the effect of the duration of AMF on drug release. UV–visible spectroscopy was performed to evaluate the effect of AMF duration on drug release from the NFA–MTX conjugate (Figure 4A). The NFA–MTX conjugate was subjected to an external magnetic field (frequency: 700–1,100 kHz) for 10, 20, and 30 min, and absorption at 304 nm was measured. Interestingly, with an increase in AMF duration, we observed an incremental release of MTX from the NFA–MTX conjugate (Figure 4A). Pure NFA did not show any representative peak at 304 nm. However, after 10 min of exposure, a distinct MTX peak was observed at 304 nm. The absorption at this time point was 0.11, which increased to 0.16 after 20 and 30 min of exposure to the magnetic field, confirming the successful release of MTX from the NFA–MTX conjugate (Figure 4A). This is one of the key findings of this research, whereby controlled drug release using MNPs is demonstrated. After incubating a known amount of MTX with NFA–SH, it was calculated that each milligram of NFA–SH was conjugated to 0.02276 mg of MTX. Furthermore, it was determined that each NFA was conjugated to nine MTX molecules and that exposure to the AMF for 30 min resulted in the release of two MTX molecules (data not shown). Quantitative release of MTX was also observed. Absorption of free MTX at fixed concentrations of 0.001, 0.01, 0.025, 0.05, 0.075, and 0.1 mg/mL was measured at 304 nm, revealing an incremental change in the absorption with increasing amounts of free MTX (Figure 4B).

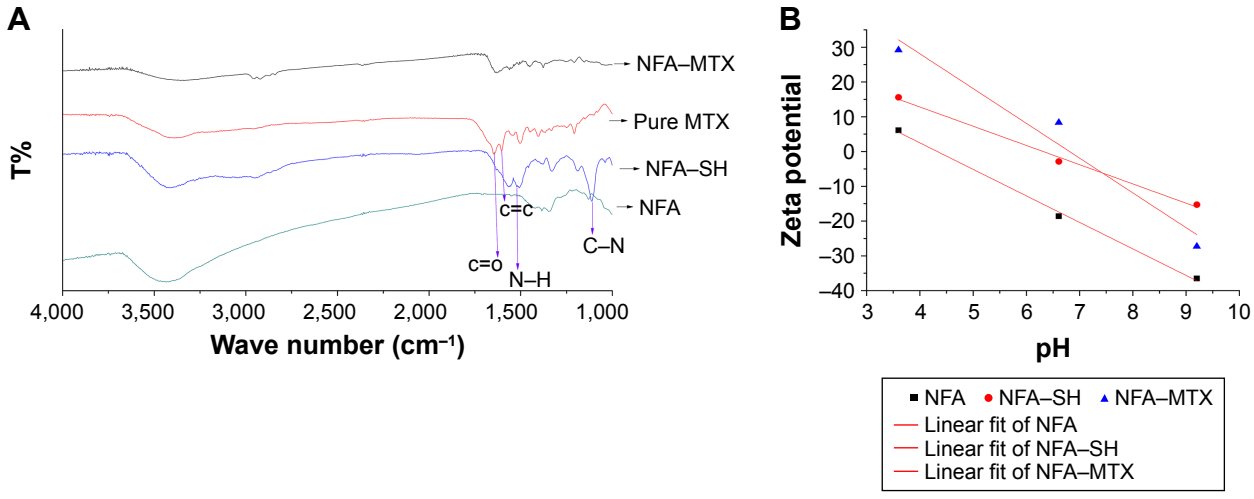

Figure 3 Conjugation of MTX onto NFAs.
Notes: (**A**) FTIR spectrum showing the presence of different functional groups in NFA–SH, pure NFA, and MTX-conjugated NFA. (**B**) Zeta potential measurement of NFA, NFA–SH, and NFA–MTX demonstrating successful conjugation of MTX onto NFA.
Abbreviations: MTX, methotrexate; NFA, Fe–Au alloy nanoparticles; FTIR, Fourier-transform infrared spectroscopy.

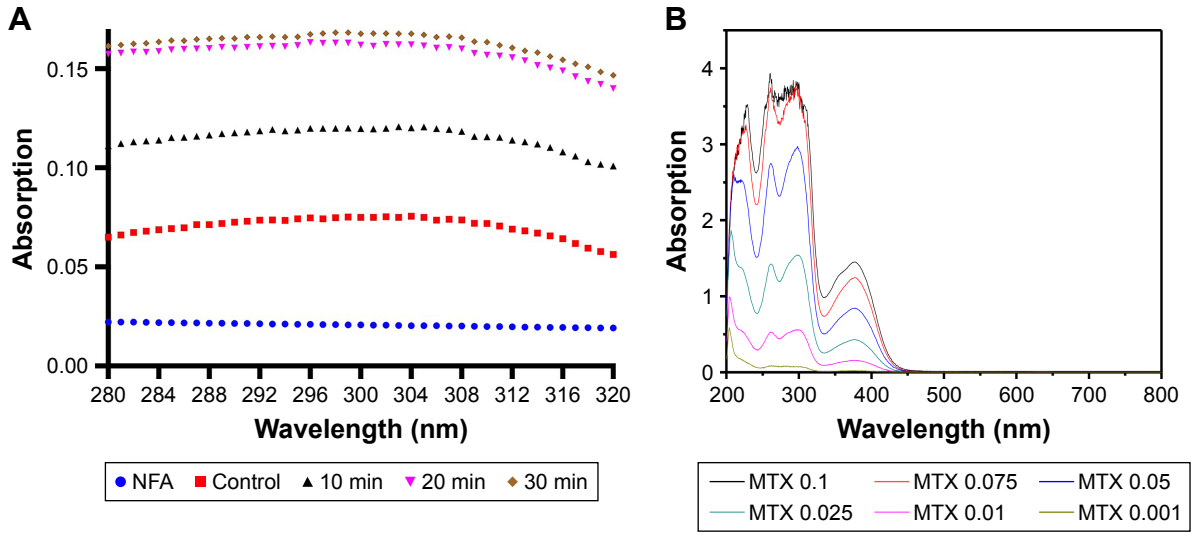

Figure 4 UV–visible spectroscopy demonstrating controlled release of MTX under AMF and its quantification.
Notes: (**A**) MTX-conjugated NFAs were subjected to AMF for 10, 20, or 30 min and absorption was measured at 304 nm. (**B**) UV–visible spectroscopy of free MTX at concentrations of 0.001, 0.01, 0.025, 0.05, 0.075, and 0.1 mg/mL.
Abbreviations: UV, ultraviolet; NFA, Fe–Au alloy nanoparticles; MTX, methotrexate; AMF, applied magnetic field.

Mechanism of NFA–SH bond cleavage and drug release

In the next step, we elucidated the mechanism of MTX release from the NFA–MTX conjugate. Previous studies have reported the generation of 1.33×10^{-16} J of heat by each NFA under the presence of an external magnetic field (frequency: 700–1,100 kHz).[33] In this study, FTIR was performed to analyze the presence of functional groups before and after the influence of an external magnetic field (Figure 5). Before heating, FTIR analysis revealed the presence of C–N stretching and N–H bending, which disappeared after the influence of the external magnetic field for 20 min (Figure 5). Since the Au–S bond energy is on the order of 45 kJ/mol (45,000/6.02/1,023 = 7.47×10^{-20} J per SH), it can be deduced that the energy provided in the form of heat was used to cleave the Au–S bonds, resulting in MTX release.

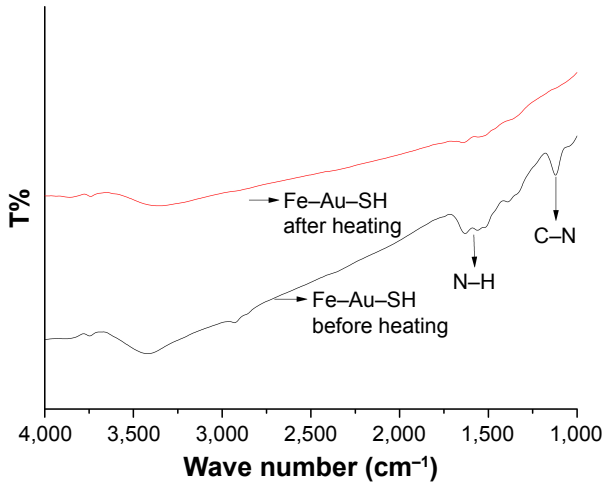

Figure 5 FTIR spectrum demonstrating the mechanism of MTX release from NFA–MTX conjugate.
Note: NFAs were functionalized with SH before and after being subjected to AMF.
Abbreviations: FTIR, Fourier-transform infrared spectroscopy; MTX, methotrexate; NFA, Fe–Au alloy nanoparticles; AMF, applied magnetic field.

Intracellular uptake

One of the major limitations of using chemotherapy drugs for cancer treatment is their nonspecific absorption by healthy stroma, leading to cell death. To counter this, we chose MTX because of its proven higher absorption by cancer cells compared to that by normal cells.[37] To evaluate the efficiency of NFA–MTX ingestion by different types of cells, ICP-MS was performed (Figure 6). ICP-MS analysis revealed a substantial difference in the ingestion rates of NFA–MTX by normal fibroblasts and cancer cells. The amount of NFA–MTX ingested by HepG2 cancer cells was 0.79 pg/cell compared to 0.53 pg/cell by the L929 fibroblasts (Figure 6). The 1.5-fold higher intake by the cancer cells compared to that by the normal fibroblasts demonstrated the specific use of NFA–MTX conjugates for cancer therapy.

As shown in the past by Kohler et al,[37] MTX uptake by breast cancer MCF-7 cells was nearly 16 folds higher compared to that by cardiomyocytes. Our results are consistent with the previous studies as we observed a 1.5-fold higher intake by HepG2 cancer cells compared to that by fibroblasts. While the ratio of drug intake by HepG2 to L929 was not as high as that observed by Kohler et al,[37] the cell lines used in the two studies may be the explanation for this difference.

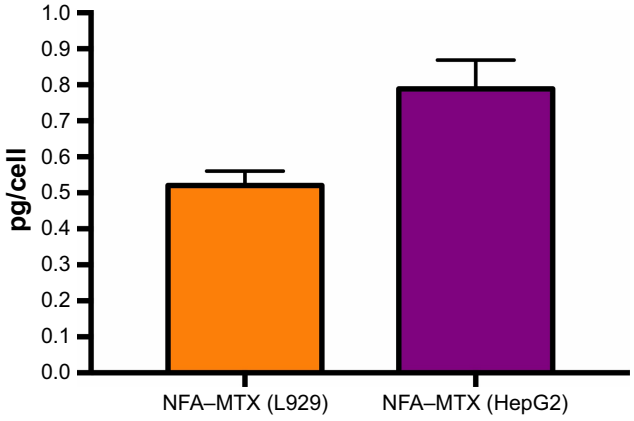

Figure 6 ICP-MS of L929 and HepG2 cells demonstrating the uptake of NFA–MTX.
Notes: L929 and HepG2 cells were incubated in 0.001 mg/mL NFA–MTX and evaluated by ICP-MS. Error bars represent mean ± SD. There is a statistical difference ($p<0.01$) between these two groups.
Abbreviations: ICP-MS, inductively coupled plasma mass spectrometry; MTX, methotrexate; NFA, Fe–Au alloy nanoparticles.

Thus, more experiments should be done to elucidate the uptake of NFA–MTX conjugates by different cancer cell lines. Nevertheless, the release of MTX via hyperthermia will evidently be ubiquitous.

Another important aspect is the position of the bond at which cleavage occurs for active MTX release. We hypothesize that after being ingested by cells, the NFAs find their way into the lysosomal compartment of the cells, wherein low pH and proteases degrade the amide bond, causing efficient release of MTX in its active form. This hypothesis is backed by similar experiments conducted by Kohler et al.[37] However, for this study, further experiments need to be conducted to confirm the efficacy of this mechanism in triggering MTX release.

Cell viability assay

All nanoparticle–drug conjugates possess a certain extent of cytotoxicity. A nanoparticle–drug conjugate with lower cytotoxicity will ensure less damage to the healthy stroma surrounding the cancer cells. Thus, to compare the cytotoxicities of NFA–MTX and unconjugated MTX, we tested NFA–MTX at concentrations ranging from 0.1 to 0.01 mg/mL and compared the results with the cytotoxicity of MTX at a fixed concentration of 0.01 mg/mL (Figure 7). HepG2 cells were incubated in different concentrations of NFA–MTX conjugates and MTX drug, and cell viability was then evaluated using the WST-8 assay. The WST-8 assay revealed a consistent decrease in cytotoxicity with the decrease in the concentration of NFA–MTX conjugates. After 24 h of incubation, for NFA–MTX, the relative absorption corresponding to cell viability was maintained at 56% at a concentration of 0.1 mg/mL and at 93% at 0.01 mg/mL (Figure 7A). In contrast, at the same concentration (0.01 mg/mL) of MTX alone, absorption was maintained at 59%, proving that at a fixed concentration, MTX is more cytotoxic to cells compared to the NFA–MTX conjugate (Figure 7A). Similar results were also obtained after 48 h of incubation. Relative absorption was maintained at 40% for NFA–MTX at 0.1 mg/mL and increased to 77% at 0.01 mg/mL. Strikingly, at the same concentration (0.01 mg/mL) of MTX alone, the absorption dropped to 37% (Figure 7B).

Our results showed that the NFA–MTX conjugates reduced the cytotoxicity of MTX by at least two folds. This implies that MTX is essentially inactive when bound to NFAs. Thus, NFA is not only crucial for controlled drug

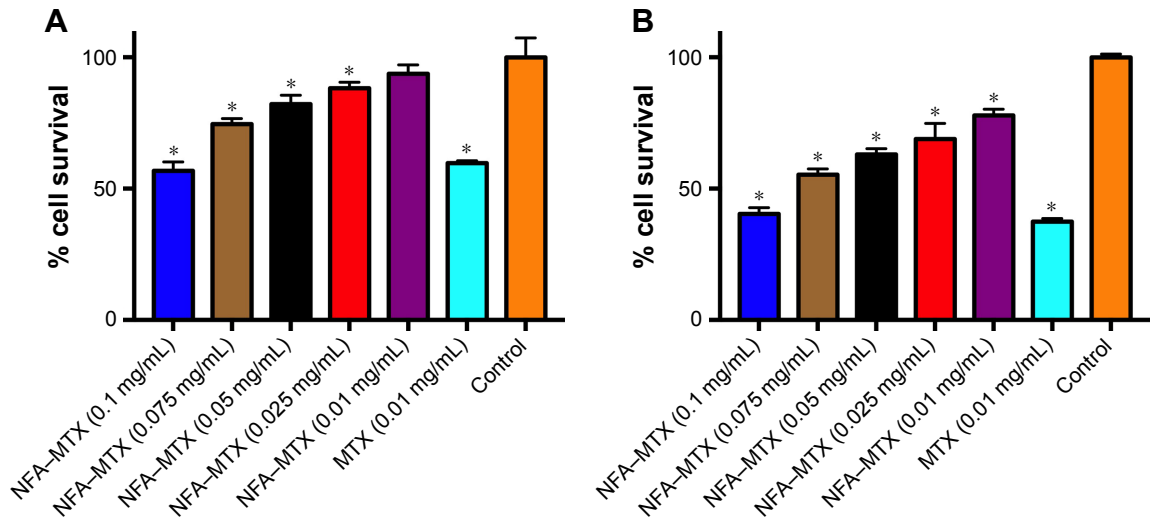

Figure 7 WST-8 assay performed to measure the relative cell viability.
Notes: HepG2 cells were cultured in different concentrations (0.1–0.01 mg/mL) of NFA–MTX or in 0.01 mg/mL MTX for (**A**) 24 h and (**B**) 48 h. Error bars represent mean ± SD.
*Statistical difference ($p<0.05$) of the group as compared to the control.
Abbreviations: MTX, methotrexate; NFA, Fe–Au alloy nanoparticles.

release, but it also ensures the safety of the cells surrounding the NFA–MTX conjugate. A small decrease in the cell viability with an increase in the NFA–MTX concentration can therefore be attributed to the NFAs.

MTX release from NFA–MTX conjugate triggers cancer cell death

To evaluate the efficiency of MTX release from NFA–MTX conjugates, after cleavage of the Au–S bond under the influence of an external magnetic field, in triggering cancer cell death, HepG2 cells were incubated in different concentrations (10, 100, and 200 µg/mL) of NFA–MTX and subjected to a magnetic field for 20 min (NFA–MTX (M)) (Figure 8). The cytotoxicity of the MTX released from NFA–MTX was also compared with that of the NFAs alone (NFA; 100 µL), NFAs under the influence of a magnetic field (NFA (M)), NFA–MTX without any magnetic field stimulation (NFA–MTX), and magnetic field alone (M). WST-8 assay was performed to evaluate the relative cell viability normalized to the cells seeded without any treatment as a control (Figure 8). Cell viability decreased by 13%, 30%, and 32% in NFA (100 µL), NFA (M) (100 µL), and NFA–MTX (10 µg/mL) (Figure 8A). Strikingly, a maximum decrease of 51% was observed in NFA–MTX (M) at 10 µg/mL. Cell viability was only 5% in NFA–MTX (M) at 100 (Figure 8B) and 200 µg/mL (Figure 8C). The cell viabilities of these two groups were the lowest among all experimental conditions, demonstrating that the MTX

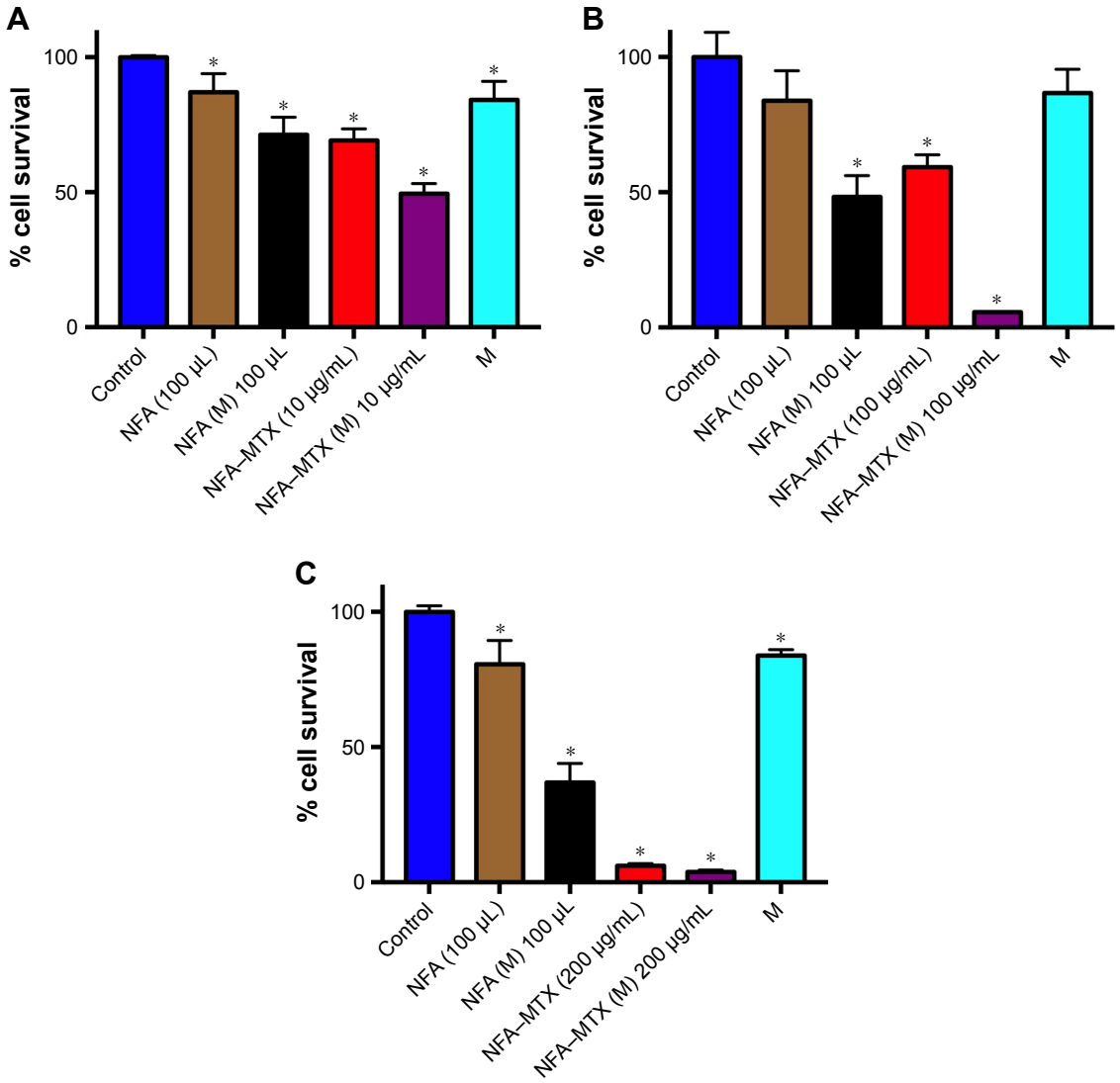

Figure 8 WST-8 assay performed to determine the effect of AMF in hyperthermia-induced drug release on cancer cell viability.
Notes: Cell viability was determined using WST-8 assay after HepG2 cells were incubated in NFA or NFA–MTX for 24 h without or with AMF (NFA (M)/NFA–MTX (M)) for 20 min with NFA–MTX at (**A**) 10 µg/mL, (**B**) 100 µg/mL, and (**C**) 200 µg/mL. A fixed concentration of NFA (100 µL) was also studied. M indicates magnetic field alone. Error bars represent mean ± SD. *Statistical difference ($p<0.05$) of the group as compared to the control.
Abbreviations: AMF, applied magnetic field; NFA, Fe–Au alloy nanoparticles; MTX, methotrexate.

released from the conjugate via hyperthermia effectively triggered cancer cell death.

Interestingly, at 200 μg/mL, NFA–MTX alone and NFA–MTX (M) both showed similar cytotoxicity, implying that a saturation level was achieved. Thus, a fine balance between the toxicity of NFA–MTX alone and of NFA–MTX (M) must be maintained to utilize this nanoparticle–drug conjugate to its true potential. However, testing would need to be carried out at more concentrations in the future to elucidate the ideal NFA–MTX concentrations for different cancer therapies. According to the results of this study, MTX-conjugated NFAs can be successfully utilized to achieve controlled drug release via hyperthermia and target cancer cells. The findings of the present study may help in engineering drug–nanoparticle conjugates for cancer therapy in achieving TDD in the field of biomedical engineering.

Conclusion

In the present study, we have engineered MTX-conjugated NFAs using 2-aminoethanethiol grafting. Our results showed that under the influence of an AMF, NFAs generate heat, which leads to the cleavage of Au–S bonds and results in MTX release. Thus, controlled drug release can be achieved by modulating the AMF. We also demonstrated the higher absorption of this drug–nanoparticle conjugate by cancer cells compared to that by normal cells, making it an ideal candidate for chemotherapy. The concentration of NFA–MTX conjugates was also optimized to ensure minimal cytotoxic effects. Finally, the ability of this conjugate to be specifically absorbed by cancer cells and trigger their death was also elucidated. This study highlights an alternate way of using hyperthermia to achieve controlled drug release. According to the results, MTX-conjugated NFAs can be successfully used to achieve controlled drug release via hyperthermia. Applications in therapeutics, biomedical engineering, and cancer research are expected.

Acknowledgments

The authors are grateful for the financial support of this research by the Ministry of Science and Technology of Taiwan (MOST 103-2221-E-027-027; MOST 104-2622-E-027-027-CC3; MOST 104-2221-E-027-061), the National Taipei University of Technology-Beijing Institute of Technology Joint Research Program (NTUT-BIT-105-3, NTUT-BIT-106-01), and partly by the Development and Reform Commission of Jilin Province, under grant number 2017C059-5.

Disclosure

The authors report no conflicts of interest in this work.

References

1. Sheth P, Sandhu H, Singhal D, Malick W, Shah N, Kislalioglu MS. Nanoparticles in the pharmaceutical industry and the use of supercritical fluid technologies for nanoparticle production. *Curr Drug Deliv*. 2012;9(3):269–284.
2. Baetke SC, Lammers T, Kiessling F. Applications of nanoparticles for diagnosis and therapy of cancer. *Br J Radiol*. 2015;88(1054):20150207.
3. De Jong WH, Borm PJA. Drug delivery and nanoparticles: applications and hazards. *Int J Nanomed*. 2008;3(2):133–149.
4. Lundqvist M, Stigler J, Elia G, Lynch I, Cedervall T, Dawson KA. Nanoparticle size and surface properties determine the protein corona with possible implications for biological impacts. *Proc Natl Acad Sci U S A*. 2008;105(38):14265–14270.
5. Navalon S, Garcia H. Nanoparticles for catalysis. *Nanomaterials*. 2016;6(7):123.
6. Choi HS, Frangioni JV. Nanoparticles for biomedical imaging: fundamentals of clinical translation. *Mol Imaging*. 2010;9(6):291–310.
7. Lim CT, Han J, Guck J, Espinosa H. Micro and nanotechnology for biological and biomedical applications. *Med Biol Eng Comput*. 2010;48(10):941–943.
8. Shi J, Votruba AR, Farokhzad OC, Langer R. Nanotechnology in drug delivery and tissue engineering: from discovery to applications. *Nano Lett*. 2010;10(9):3223–3230.
9. Vieira S, Vial S, Reis RL, Oliveira JM. Nanoparticles for bone tissue engineering. *Biotechnol Prog*. 2017;33(3):590–611.
10. Craig GA, Allen PJ, Mason MD. Synthesis, characterization, and functionalization of gold nanoparticles for cancer imaging. *Methods Mol Biol*. 2010;624:177–193.
11. Naik K, Chatterjee A, Prakash H, Kowshik M. Mesoporous TiO_2 nanoparticles containing Ag ion with excellent antimicrobial activity at remarkable low silver concentrations. *J Biomed Nanotechnol*. 2013;9(4):664–673.
12. Zhang WH, Hu XX, Zhang XB. Dye-doped fluorescent silica nanoparticles for live cell and in vivo bioimaging. *Nanomaterials (Basel)*. 2016;6(5):E81.
13. Aires A, Ocampo SM, Simoes BM, et al. Multifunctionalized iron oxide nanoparticles for selective drug delivery to CD44-positive cancer cells. *Nanotechnology*. 2016;27(6):065103.
14. McBain SC, Yiu HHP, Dobson J. Magnetic nanoparticles for gene and drug delivery. *Int J Nanomedicine*. 2008;3(2):169–180.
15. Yu Z, Ma X, Yu B, Pan Y, Liu Z. Synthesis and characterization of ZnS:Mn/ZnS core/shell nanoparticles for tumor targeting and imaging in vivo. *J Biomater Appl*. 2013;28(2):232–240.
16. Siegel RL, Miller KD, Jemal A. Cancer statistics, 2016. *CA Cancer J Clin*. 2016;66(1):7–30.
17. Witsch E, Sela M, Yarden Y. Roles for growth factors in cancer progression. *Physiology (Bethesda)*. 2010;25(2):85–101.
18. Li S, Qin X, Chai S, Qu C, Wang X, Zhang H. Modulation of E-cadherin expression promotes migration ability of esophageal cancer cells. *Sci Rep*. 2016;6:21713.
19. Bhardwaj V, Hariharan S, Bala I, et al. Pharmaceutical aspects of polymeric nanoparticles for oral drug delivery. *J Biomed Nanotechnol*. 2005;1(3):235–258.
20. Liu Y, Li J, Liu F, Feng L, Yu D, Zhang N. Theranostic polymeric micelles for the diagnosis and treatment of hepatocellular carcinoma. *J Biomed Nanotechnol*. 2015;11(4):613–622.
21. Qi X, Qin J, Fan Y, Qin X, Jiang Y, Wu Z. Carboxymethyl chitosan-modified polyamidoamine dendrimer enables progressive drug targeting of tumors via pH-sensitive charge inversion. *J Biomed Nanotechnol*. 2016;12(4):667–678.
22. Yang J, Shimada Y, Olsthoorn RC, Snaar-Jagalska BE, Spaink HP, Kros A. Application of coiled coil peptides in liposomal anticancer drug delivery using a zebrafish xenograft model. *ACS Nano*. 2016;10(8):7428–7435.

23. Ulbrich K, Hola K, Subr V, Bakandritsos A, Tucek J, Zboril R. Targeted drug delivery with polymers and magnetic nanoparticles: covalent and noncovalent approaches, release control, and clinical studies. *Chem Rev*. 2016;116(9):5338–5431.
24. Li Y, Li N, Pan W, Yu Z, Yang L, Tang B. Hollow mesoporous silica nanoparticles with tunable structures for controlled drug delivery. *ACS Appl Mater Interfaces*. 2017;9(3):2123–2129.
25. Cui T, Liang JJ, Chen H, et al. Performance of doxorubicin-conjugated gold nanoparticles: regulation of drug location. *ACS Appl Mater Interfaces*. 2017;9(10):8569–8580.
26. Wahajuddin, Arora S. Superparamagnetic iron oxide nanoparticles: magnetic nanoplatforms as drug carriers. *Int J Nanomedicine*. 2012;7:3445–3471.
27. Dobson J. Gene therapy progress and prospects: magnetic nanoparticle-based gene delivery. *Gene Ther*. 2006;13(4):283–287.
28. Estelrich J, Sanchez-Martin MJ, Busquets MA. Nanoparticles in magnetic resonance imaging: from simple to dual contrast agents. *Int J Nanomedicine*. 2015;10:1727–1741.
29. Sivakumar B, Aswathy RG, Sreejith R, et al. Bacterial exopolysaccharide based magnetic nanoparticles: a versatile nanotool for cancer cell imaging, targeted drug delivery and synergistic effect of drug and hyperthermia mediated cancer therapy. *J Biomed Nanotechnol*. 2014;10(6):885–899.
30. Fatima H, Kim K-S. Magnetic nanoparticles for bioseparation. *Korean J Chem Eng*. 2017;34(3):589–599.
31. Song AS, Najjar AM, Diller KR. Thermally induced apoptosis, necrosis, and heat shock protein expression in 3D culture. *J Biomech Eng*. 2014;136(7):doi: 10.1115/1.4027272.
32. Khan VR, Brown IR. The effect of hyperthermia on the induction of cell death in brain, testis, and thymus of the adult and developing rat. *Cell Stress Chaperones*. 2002;7(1):73–90.
33. Chung R-J, Wang H-Y, Wu K-T. Preparation and characterization of Fe-Au alloy nanoparticles for hyperthermia application. *J Med Biol Eng*. 2014;34(3):251–255.
34. Azizi S, Mohamad R, Bahadoran A, et al. Effect of annealing temperature on antimicrobial and structural properties of bio-synthesized zinc oxide nanoparticles using flower extract of *Anchusa italica*. *J Photochem Photobiol B*. 2016;161:441–449.
35. Krishnamurthy S, Esterle A, Sharma NC, Sahi SV. Yucca-derived synthesis of gold nanomaterial and their catalytic potential. *Nanoscale Res Lett*. 2014;9(1):627.
36. He X, Shi H. Size and shape effects on magnetic properties of Ni nanoparticles. *Particuology*. 2012;10(4):497–502.
37. Kohler N, Sun C, Wang J, Zhang M. Methotrexate-modified superparamagnetic nanoparticles and their intracellular uptake into human cancer cells. *Langmuir*. 2005;21(19):8858–8864.